

Three-Dimensional Blood Vessel Segmentation and Centerline Extraction based on Two-Dimensional Cross-Section Analysis

RAHUL PRASANNA KUMAR,^{1,2} FRITZ ALBREGTSEN,^{2,3} MARTIN REIMERS,² BJØRN EDWIN,^{1,4} THOMAS LANGØ,⁵
and OLE JAKOB ELLE^{1,2}

¹The Intervention Centre, Oslo University Hospital, Sognsvannsveien 20, 0372 Oslo, Norway; ²Department of Informatics, University of Oslo, Gaustadalléen 23 B, 0373 Oslo, Norway; ³Institute for Cancer Genetics and Informatics, Oslo University Hospital, Sognsvannsveien 20, 0372 Oslo, Norway; ⁴Faculty of Medicine, University of Oslo, Klaus Torgårds vei 3, 0372 Oslo, Norway; and ⁵Medical Technology, SINTEF, Olav Kyrres Gate 9, MTF5, Trondheim, Norway

(Received 4 June 2014; accepted 5 November 2014)

Associate Editor Joel D. Stitzel oversaw the review of this article.

Abstract—The segmentation of tubular tree structures like vessel systems in volumetric datasets is of vital interest for many medical applications. In this paper we present a novel, semi-automatic method for blood vessel segmentation and centerline extraction, by tracking the blood vessel tree from a user-initiated seed point to the ends of the blood vessel tree. The novelty of our method is in performing only two-dimensional cross-section analysis for segmentation of the connected blood vessels. The cross-section analysis is done by our novel single-scale or multi-scale *circle enhancement* filter, used at the blood vessel trunk or bifurcation, respectively. The method was validated for both synthetic and medical images. Our validation has shown that the cross-sectional centerline error for our method is below 0.8 pixels and the Dice coefficient for our segmentation is $80\% \pm 2.7\%$. On combining our method with an optional active contour post-processing, the Dice coefficient for the resulting segmentation is found to be $94\% \pm 2.4\%$. Furthermore, by restricting the image analysis to the regions of interest and converting most of the three-dimensional calculations to two-dimensional calculations, the processing was found to be more than 18 times faster than Frangi *vesselness* with thinning, 8 times faster than user-initiated active contour segmentation with thinning and 7 times faster than our previous method.

Keywords—Blood vessel segmentation, Centerline extraction, Vessel tracking, Multi-scale analysis and circle enhancement filter.

INTRODUCTION

Many clinical practices rely on angiography in multiple imaging modalities. This leads to an increasing need for visualization and segmentation of blood vessels. Analysis of blood vessel morphology is very important in many clinical applications for diagnosis, planning and navigation. This is especially important for planning liver resections and navigation of catheter-based interventions. Catheter tracking require precise knowledge of the blood vessels for accurate positioning of stents and valves.

Manual segmentation of blood vessels is impractical as they present very complex 3D structures, which makes an automatic or semi-automatic segmentation important. In the literature, many papers are dealing with blood vessel segmentation.^{10,15} Conventional blood vessel segmentation methods can be classified as top-down or bottom-up approaches. In top-down approaches, the process starts from single or multiple user-initiated seed points and iteratively merges nearby structures or regions based on a predefined condition. In bottom-up approaches, a predefined condition for blood vessel segmentation is evaluated at each and every voxel of the input image, not requiring any seed point initializations from the user.

Typical top-down methods include region growing and deformable models. Two major conditions looked for in region growing methods are intensity value similarity and spatial proximity.^{22,23} Region growing methods also include an initial thresholding. Deformable model methods include active contours or snakes, level sets and wave-front propagation.^{1,8,9,17,19} These methods work on iteratively adjusting the initial user

Address correspondence to Rahul Prasanna Kumar, The Intervention Centre, Oslo University Hospital, Sognsvannsveien 20, 0372 Oslo, Norway. Electronic mail: rahul.kumar@rr-research.no

set contour to fit to the blood vessel structure. The major disadvantages of these methods are that there is little use of structure information leading to high chance of leakage, and also that iteratively modifying the contour is very time consuming.

Typical bottom-up methods are based on local shape descriptors or tube detection filters.^{4,5,11,21} The radius for tube detection varies, but following the concepts of scale-space theory,¹⁶ the response of a tubular filter is maximal if the scale fits the object size. Conventional tube detection filters try to identify the tubular objects at different scales and combine all responses into one multi-scale response. The major disadvantages of such methods are that they are computationally very expensive, due to their processing of each and every voxel and its neighborhood in the image at several scales.

Along with segmentation, a centerline extraction of these blood vessels is also important. An extracted centerline could be used for fast registration of blood vessels and updating blood vessel models obtained intraoperatively.^{13,20} We have earlier proposed a centerline extraction method that uses our *modified multiscale vesselness* equation.¹² Our earlier method was faster than the conventional *vesselness* method by performing the modified *vesselness* only within regions of interest; however, this was still not fast enough, as it required prior calculation of whole image Hessian.

In this paper, we present a novel blood vessel segmentation and centerline extraction method incorporating both top-down and bottom up approaches. The main aim of this method is to provide the user with a fast and easy to use blood vessel segmentation method, which has the potential to be used for updating models during intra-operative procedures. The proposed method is semi-automatic and works by processing a single 2D blood vessel cross-section at a time and tracking the connected blood vessel tree to its end points. The final 3D blood vessel segmentation is calculated by combining all the tracked 2D vessel cross-sections.

METHODS

Our proposed method focuses on segmenting the 3D connected blood vessels by tracking their cross-sections from a user-initialized seed to the blood vessel ends. The user initializes the tracking by setting a seed point, a direction seed point and an approximate blood vessel cross-section radius at the seed point.

In this section we describe the proposed method, which is divided into four parts: (1) cross-section image, (2) preprocessing for cross-section image analysis, (3) bifurcation detection, and (4) circle enhancement filter. In the first part, we describe how the cross-section image is calculated at a seed point and its

corresponding cross-sections. In the second part, we describe all the preprocessing steps required for further cross-section analysis. In the third part, we describe how a cross-section is classified as a bifurcation. In the fourth, we describe our novel circle enhancement filter, which is used enhancing the blood vessel cross-section and subsequent centerline extraction. Finally, we describe an optional post-processing step that allows the user to modify the output, so that the eventual segmentation gaps are filled properly.

Cross-Section Image

At the beginning, the tracking direction of the connected blood vessel of interest is estimated as the vector connecting the seed point and the direction seed point,

$$T = (x_s - x_d)\hat{i} + (y_s - y_d)\hat{j} + (z_s - z_d)\hat{k} \quad (1)$$

$$\hat{i} = \frac{T}{|T|} \quad (2)$$

where T is the tracking direction, (x_s, y_s, z_s) is the seed point, (x_d, y_d, z_d) is the direction seed and \hat{i} is the unit vector along the tracking direction.

The tracking direction is used only at the seed point to initialize the direction of segmentation. At the seed, the tracking direction is set as the vessel direction of flow and its cross vectors are set as the approximate vectors representing the cross-section of the blood vessel. However, an Eigen analysis of the Hessian matrix is calculated for precise information of the vessel cross-section vectors. For the subsequent cross-sections along a trunk, the next possible center pixel or the center candidate is determined by moving along the vessel direction from the previous center position.

Eigen analysis can geometrically interpret the second order derivatives of an image at each point. The second order differential quantity for a volume $I(x, y, z)$ with a Gaussian convolution $g_\sigma(x, y, z)$, is given by the indefinite Hessian matrix,^{4,5,21}

$$H(x, y, z; \sigma) = \begin{bmatrix} I * \frac{\partial^2 g_\sigma}{\partial x^2} & I * \frac{\partial^2 g_\sigma}{\partial x \partial y} & I * \frac{\partial^2 g_\sigma}{\partial x \partial z} \\ I * \frac{\partial^2 g_\sigma}{\partial y \partial x} & I * \frac{\partial^2 g_\sigma}{\partial y^2} & I * \frac{\partial^2 g_\sigma}{\partial y \partial z} \\ I * \frac{\partial^2 g_\sigma}{\partial z \partial x} & I * \frac{\partial^2 g_\sigma}{\partial z \partial y} & I * \frac{\partial^2 g_\sigma}{\partial z^2} \end{bmatrix} \quad (3)$$

where

$$g_\sigma(x, y, z) = \frac{1}{(\sigma\sqrt{2\pi})^3} e^{-(x^2+y^2+z^2)/2\sigma^2} \quad (4)$$

and σ is the scale parameter set according to the radius of the blood vessel. At the initial seed point, the user defined initial radius is set as the σ , and for the subsequent cross-sections analysis, the previous cross-section radius is set as the σ .

Let the eigenvalues of the Hessian matrix H , be λ_1 , λ_2 and λ_3 , and their respective normalized eigenvectors be represented by \vec{v}_1 , \vec{v}_2 and \vec{v}_3 . On sorting the eigenvalues as $|\lambda_1| \leq |\lambda_2| \leq |\lambda_3|$, the eigenvector \vec{v}_1 represents the vessel direction and the eigenvectors \vec{v}_2 and \vec{v}_3 represent the vessel cross-section vectors. These vessel cross-section vectors are used to create the vessel cross-section image, as shown in Fig. 1. The vessel cross-section image is found by interpolating at a discrete set of points along the 2D plane represented by the two cross vectors, \vec{v}_2 and \vec{v}_3 .

Preprocessing for Cross-Section Image Analysis

Before moving into the cross-section analysis, some preprocessing steps have to be performed for calculating the vessel cross-section border, radius and local threshold. These preprocessing steps help understanding

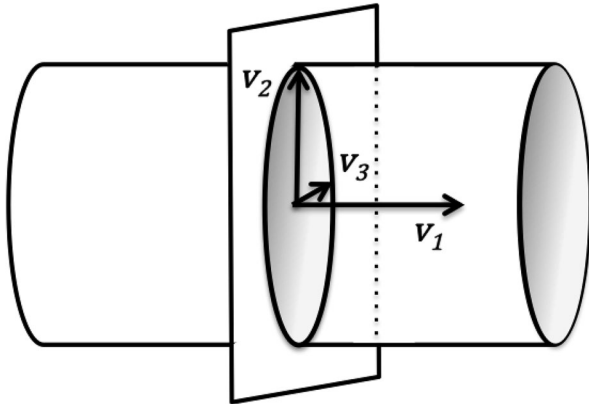


FIGURE 1. Vessel cross-section image made using the vessel cross vectors \vec{v}_2 and \vec{v}_3 .

the structure at the cross-section and thus in segmenting the blood vessel itself.

The border of the vessel cross-section is found by applying a Canny edge detection filter on the cross-section image, as the blood vessel intensity is different from that of its surroundings.³ 2D Gaussian smoothing filter is applied at the beginning of the Canny filter to smooth out noise. The variance of the Gaussian is proportional to the square of previous radius or the initial user-set radius. Figure 2 shows the border of the blood vessel cross-section after applying the Canny edge detection method. Each border pixel obtained represents the discrete border contour of the vessel cross-section.

An approximate diameter of the cross-section is calculated by taking the maximum of the diameters along the perpendicular vectors \vec{v}_2 and \vec{v}_3 , from the seed to the cross-section border, as shown in Fig. 2. Finally, the local threshold at the vessel cross-section is also found by averaging all the blood vessel cross-section intensities along the border of the vessel cross-section.

Bifurcation Detection

After performing the preprocessing steps, each of the vessel cross-section images are checked to determine if it is a bifurcation. The contour of a vessel bifurcation cross-section is very different from the contour of a vessel trunk cross-section. Figure 3 illustrates difference in the shape of the vessel cross-sections between trunk and bifurcation. By calculating the shape descriptors: compactness and radius variance, we can identify bifurcating vessel cross-sections.¹⁸

Compactness is a measure of how circular a given contour is. It can be defined as

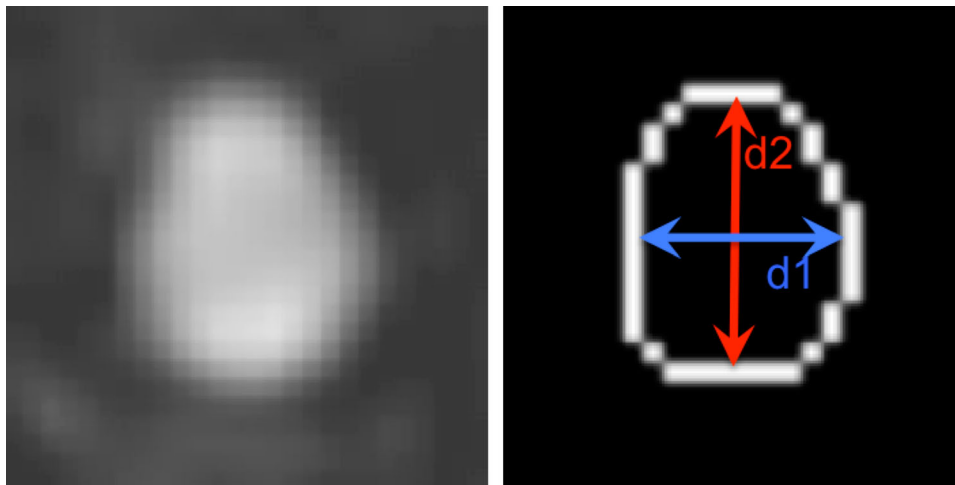


FIGURE 2. Right: Vessel cross-section image, and Left: Canny edge of the vessel cross-section and the two diameters, d_1 and d_2 , along the perpendicular vectors \vec{v}_2 and \vec{v}_3 , from the seed.

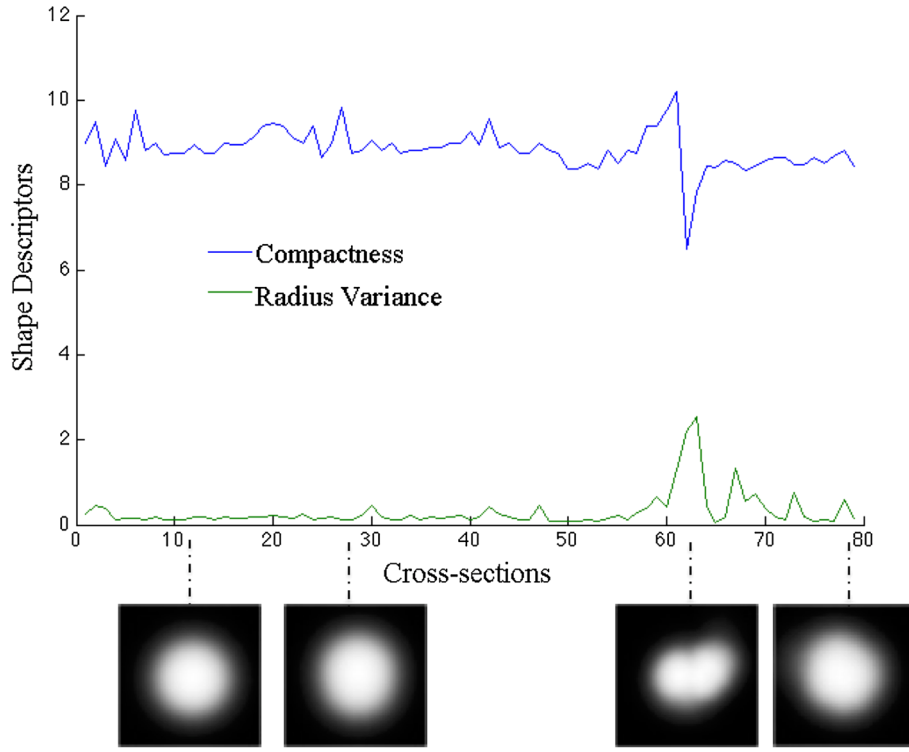


FIGURE 3. Shape descriptor values at various cross-section images along a blood vessel.

$$\text{Compactness} = \frac{P^2}{A} \quad (5)$$

where P is the perimeter of the vessel cross-section shape and A is the area of vessel cross-section. Radius variance is the variance in distance from the center candidate to the border points or vessel cross-section contour.

Whenever there is a sudden increase above a certain threshold or a sudden change in the shape descriptors (compactness and radius variance), the corresponding cross-sections are analyzed as bifurcation cross-sections. Figure 3 illustrates how the shape descriptor values change as the cross-section changes from vessel trunk to the vessel bifurcation. The sudden change in the shape descriptors resembles the change in vessel cross-section border, signifying bifurcation.

Circle Enhancement Filter

On determining whether the vessel cross-section is part of a vessel trunk or a vessel bifurcation, the process goes forward in enhancing the structure accordingly and finding the center of the cross-section. We have implemented a novel circle enhancement or “*circleness*” filter, which enhances circular structures in the image and provides a good Gaussian profile for the

output intensity. The filter adopts the scale space approach with the possibility of performing the operation in single or multiscale.

In the proposed method, a single scale approach is used to enhance the cross-section at vessel trunks, while the multiscale space approach is used to enhance the cross-section at vessel bifurcations. This makes the bifurcation detection step a very crucial step.

Our *circleness* filter is based on 2D Eigen analysis on the 2D Hessian matrix computed at each pixel of the vessel cross-section image. Similar to Eq. 3, the 2D Hessian matrix is given by,

$$H_{2D}(x, y; \sigma) = \begin{bmatrix} I_{2D} * \frac{\partial^2 g_{2D\sigma}}{\partial^2 x} & I_{2D} * \frac{\partial^2 g_{2D\sigma}}{\partial x \partial y} \\ I_{2D} * \frac{\partial^2 g_{2D\sigma}}{\partial y \partial x} & I_{2D} * \frac{\partial^2 g_{2D\sigma}}{\partial^2 y} \end{bmatrix} \quad (6)$$

where I_{2D} is the vessel cross-section image, $g_{2D\sigma}$ is the 2D Gaussian filter and σ is the scale parameter set according to the vessel cross-section radius, which is found at the preprocessing step.

Let λ_{2D1} and λ_{2D2} be the eigenvalues from the 2D Hessian matrix. These eigenvalues are used to understand the structural information of at each pixel of the cross-section image. The *circleness* filter is formulated with the knowledge that both the eigenvalues will be high at the center of the cross-section as the cross-section is near circular in nature. After sorting

the eigenvalues ($|\lambda_{2D1}| \leq |\lambda_{2D2}|$), we have coined a *circleness* ratio

$$C_R = \frac{|\lambda_{2D1} + \lambda_{2D2}|}{\left| |\lambda_{2D2}| - |\lambda_{2D1}| \right|} \quad (7)$$

Our novel *circleness* equation at a single scale using the *circleness* ratio C_R is

$$C = \left(1 - e^{-(C_R k)^2}\right) \left(1 - e^{-\frac{S^2}{2k^2}}\right) \quad (8)$$

where k affects the rate of increase of the Gaussian profile of the *circleness* filter, while S is the Frobenius matrix norm of the Hessian,

$$S = \sqrt{\lambda_{2D1}^2 + \lambda_{2D2}^2} \quad (9)$$

which reduces the effect of noise in the filtered output.

For more efficient processing, we apply our *circleness* filter only inside the vessel cross-section region. The region of interest is determined by applying the local threshold found in the preprocessing step. Figure 4a shows the single scale *circleness* filter output on a vessel trunk cross-section image. The single peak obtained from the single scale *circleness* filter applied to a vessel trunk cross-section is the center of that cross-section. Moving along the vessel direction \vec{v}_1 from the current center, we find the next possible center or the next center candidate for the next cross-section of the vessel trunk.

At the bifurcation cross-section, we apply the multiscale *circleness* filter. This allows determination of multiple peaks, where each corresponds to a bifurcating vessel. The multiscale *circleness* is formulated as,

$$C_{\text{multi}} = \max_{\sigma_{\min} \leq \sigma \leq \sigma_{\max}} C(\sigma) \quad (10)$$

where σ_{\min} is the minimum radius and σ_{\max} is the maximum radius. σ_{\max} is set as the radius of the cross-section and, σ_{\min} is set as one-third the value of σ_{\max} for detecting smaller bifurcations of up to one-third the size of the radius.

Figure 4b shows the multiscale *circleness* filter output with multiple centers at the vessel bifurcation cross-section image, where each center corresponds to a different bifurcating vessel. Each center found at the bifurcation cross-section is set as a new seed for the whole process to start again.

At the vessel cross-section, the immediate surrounding 3D neighborhood is also checked and added as part of the vessel, if they fall within the local vessel threshold. This helps in reducing the gaps that might be caused by processing 2D slices along a 3D blood vessel. The vessel cross-section tracking finally stops, when the newly found center candidate falls outside the connected blood vessel region.

While tracking through the blood vessel, the *circleness* filter output at each vessel cross-section is added into its corresponding 3D voxel in the final segmentation output. Thus, when the whole connected blood vessel tree is tracked, the method simultaneously produces the complete 3D blood vessel segmentation output and the extracted centerline.

Post-processing

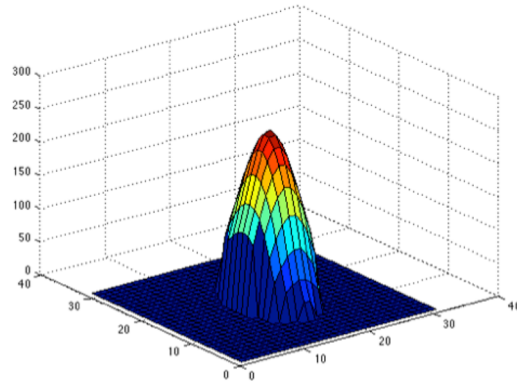
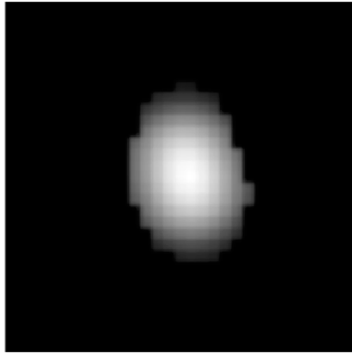
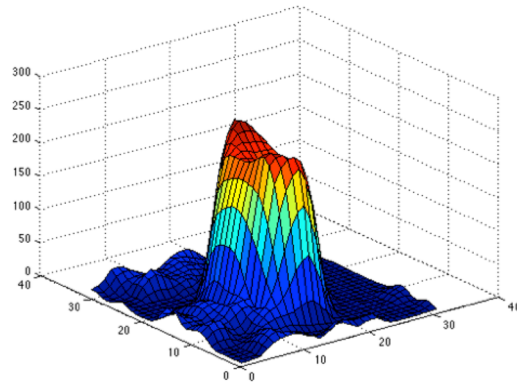
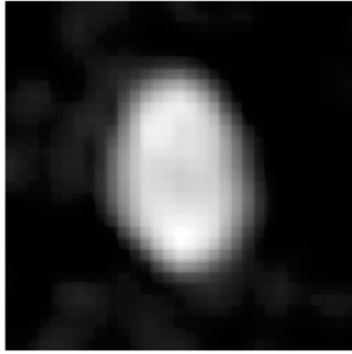
The initial 3D blood vessel segmentation result is obtained after the vessel cross-section tracking comes to a stop by reaching all the blood vessel end-points. The user then has an option to perform a post-processing, where the initial blood vessel segmentation output is set as a seed volume or contour for an active contour evolution.²⁴ The user has the option to set the region of interest and the processing intensity range. Adjusting lower and upper threshold values sets the intensity range, and the curve within the intensity range can be low-pass filtered for smooth propagation of the contour. Finally, the user also has to set values for external and internal forces governing the flow of the contour, before starting the evolution. On completing the evolution, the final 3D blood vessel segmentation is obtained, which has a smooth surface, well fitted to the original blood vessel.

RESULTS

The proposed method was applied on a set of eight images: four synthetic blood vessel images and four medical images. The synthetic images used for our validation were made by a method proposed by Galarreta-Valverde *et al.*, which is an extension of the traditional Lindenmayer system (L-system) that generates synthetic 3D blood vessels by adding stochastic rules, and they were downloaded from Galarreta-Valverde's web-database of synthetic images.⁶ These synthetic images were chosen, as they resemble blood vessels from medical images to a great extent. All the medical and synthetic images were resampled to $1 \text{ mm} \times 1 \text{ mm} \times 1 \text{ mm}$ voxels to obtain an isotropic image resolution that is good for structural analysis.

Figure 5 shows the synthetic blood vessel images and various outputs obtained using different methods. The first column shows all the synthetic blood vessel images (Image1–4) used in our study. The second column shows the 3D models made from Frangi *vesselness*.⁵ In the third column, the 3D segmented output from the active contour method with a user-initiated seed point is shown.²⁴ The fourth column shows the 3D models made from blood vessel segmentation using our proposed method without the

(a)



(b)

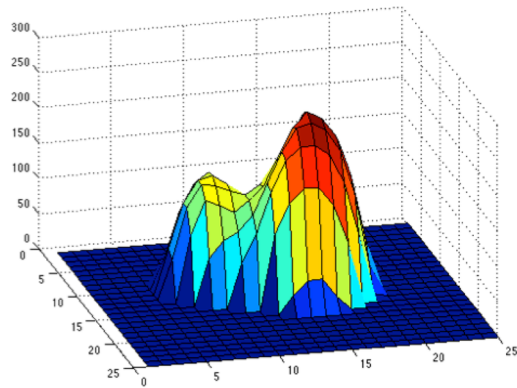
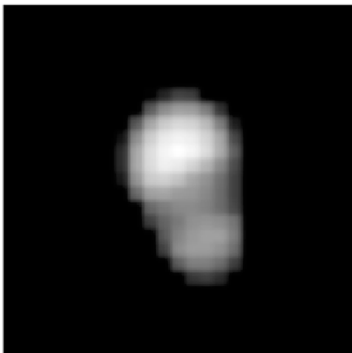
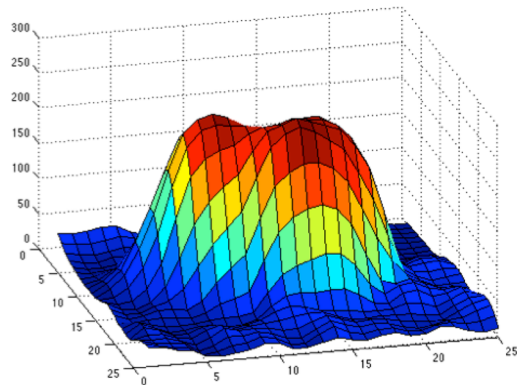
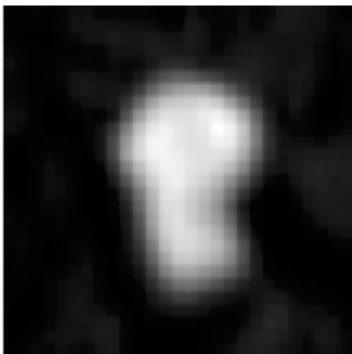


FIGURE 4. (a) Top row: Input vessel trunk cross-section image and its 3D intensity plot, Bottom row: Single scale *circleness* image of trunk cross-section image and its 3D intensity plot; (b) Top row: Input vessel bifurcation cross-section image and its 3D intensity plot, Bottom row: Multi-scale *circleness* image of bifurcation cross-section image and its 3D intensity plot.

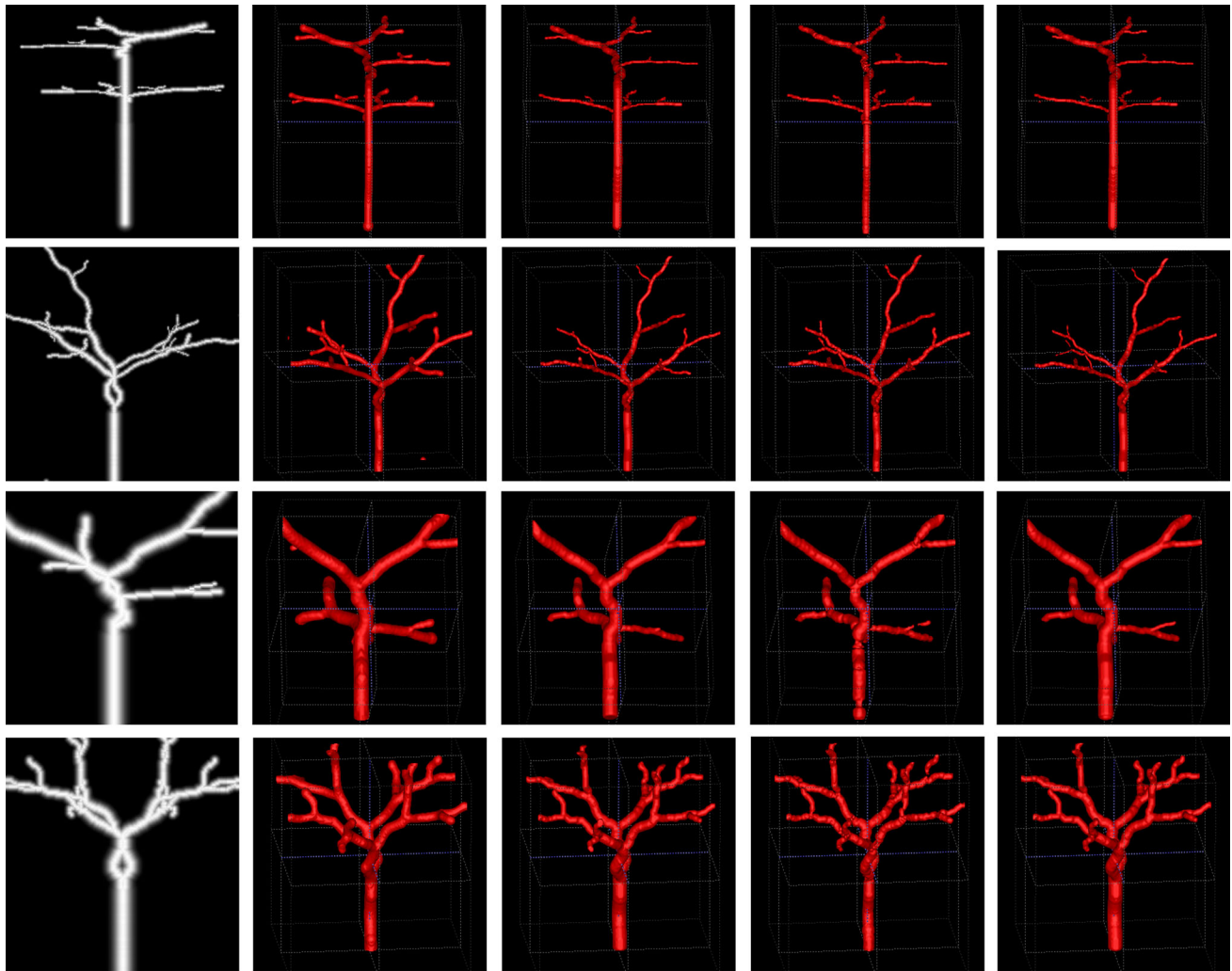


FIGURE 5. First column: Maximum Intensity Projection (MIP) images of input synthetic images (Images1–4); Second column: 3D view of blood vessel segmentation obtained using Frangi *vesselness*; Third column: 3D view of blood vessel segmentation obtained using semi-automatic active contour segmentation; Fourth column: 3D view of blood vessel segmentation obtained using our proposed method without post-processing step; Last column: 3D view of blood vessel segmentation obtained using our proposed method with post-processing step.

optional post-processing step, and the segmentation result with post-processing step is shown on the last column. We did not consider adding noise in the synthetic images as our method expects that a blood vessel with contrast will have higher intensity inside than outside of the vessel. Also, our method works by tracking the blood vessel only from within the blood vessel, without considering the outside noise.

Figure 6 shows the medical images used in our study and their corresponding outputs. All the medical images (Image5–8) shown in the first column are contrast enhanced magnetic resonance angiogram images. The centerlines extracted using the proposed method are shown in the second column. Lastly in Fig. 6, the 3D model views from the blood vessel segmentation performed using Frangi *vesselness* with thresholding,^{5,7} active contour segmentation²⁴ and the proposed

method are shown in the third, fourth and last column, respectively. For medical images, the thresholding for Frangi *vesselness* is done using maximum entropy thresholding.⁷ The entropy-based thresholding method is selected as it is shown to give better results when compared to other similar thresholding methods.² The seed for the active contour segmentation is a sphere with diameter of 5 voxels and center at the same position as that of the corresponding seed for the proposed method.

Processing Time

All blood vessel images, both synthetic and medical, used in our study were segmented on a MacBook Pro with 2 GHz Intel Core i7 processor and 8 GB 1600 MHz DDR3 RAM. We compared the processing

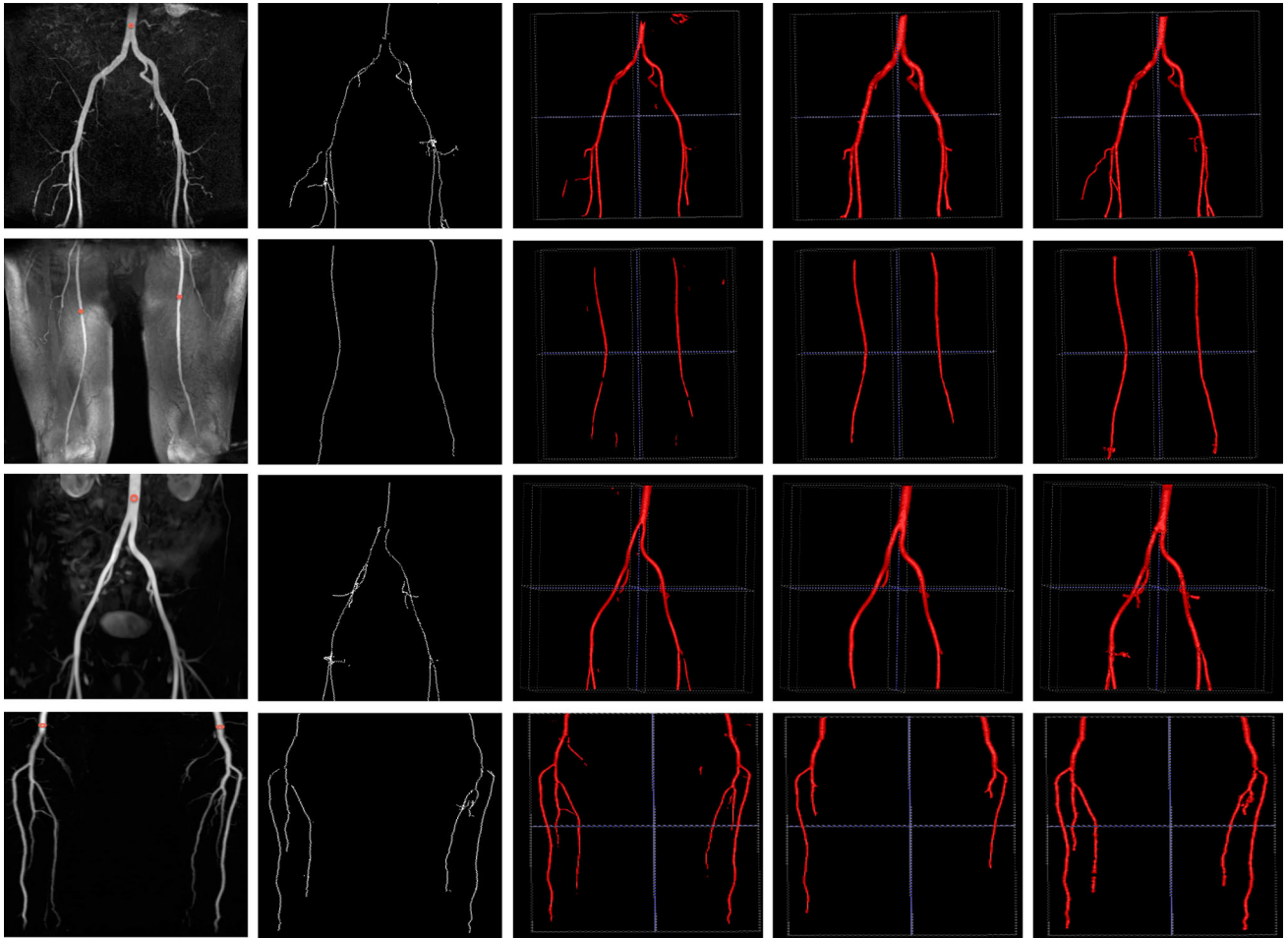


FIGURE 6. First column: Maximum Intensity Projection (MIP) images of input medical images (Images5–8), with red circles indicating the seed points; Second column: MIP images of centerlines obtained using our proposed method; Third column: 3D volume view of blood vessel segmentation obtained using Frangi *vesselness* and max entropy thresholding; Fourth column: 3D volume view of blood vessel segmentation obtained using seed initiated active contour segmentation; Last column: 3D volume view of blood vessel segmentation obtained using our proposed method without post-processing step.

TABLE 1. Processing time taken for centerline extraction using, Frangi *vesselness* with 3D thinning (*F.V.+T.*),^{5,14} seed initiated active contour with 3D thinning (*A.C.+T.*),^{14,24} our earlier method¹² and our current proposed method.

Data, size	<i>F.V.+T.</i> (s)	<i>A.C.+T.</i> (s)	Earlier (s)	Curr. (s)
Image1, 345 × 345 × 345	899	441	434	26
Image2, 300 × 300 × 300	604	225	270	19
Image3, 150 × 150 × 150	71	36	36	9
Image4, 225 × 225 × 225	254	105	109	23
Image5, 384 × 384 × 82	321	132	96	28
Image6, 352 × 384 × 95	274	107	32	12
Image7, 356 × 330 × 124	406	157	149	19
Image8, 272 × 499 × 88	198	151	88	26

time for segmenting the blood vessels from the 8 images by different methods. Table 1 shows the processing time taken for centerline extraction by Frangi *vesselness* with thinning,^{5,7,14} active contour segmentation with thinning, our own earlier method for

centerline extraction¹² and our proposed method. The thinning for both Frangi *vesselness* and active contour segmentation was performed using Lee's method,¹⁴ where the 3D neighborhood of each foreground voxel is checked for thinning. Our proposed method is shown to be on average more than 18 times faster than Frangi *vesselness* with thinning, 8 times faster than active contour segmentation and more than 7 times faster than our earlier method¹² for centerline extraction.

Centerline Validation

Centerline validation is performed by finding the error between the ground-truth center and the center, from the proposed method at each vessel cross-section. Making a reliable manual ground-truth center for each and every vessel cross-section is a time consuming task for humans. An alternative is to find the geometric

center of the vessel cross-section, which is calculated by performing Hough circle detection, as the blood vessel cross-sections resemble circles. The Hough circle center will correspond to the center of the vessel cross-section even when the cross-section is elliptical in shape.

The center error is calculated by finding the Euclidean distance between the Hough circle center and the center calculated by the proposed method. Figure 7 shows the mean center error at vessel cross-sections of all synthetic and medical images at various radius, and the standard deviation between images. The center error decreases with increasing radius, where the center error is the highest at 1 pixel radius with 0.75 pixels error and least at 7 pixels radius with 0.09 pixels error.

Segmentation Validation

Ground-truth data for the images are necessary for validating the segmentation methods. In our study, we only made ground-truth data for synthetic images and the segmentation validation was performed only on these images. A simple thresholding is sufficient to create the ground-truth images for synthetic images, as there is no information outside the vessel regions.

In our study, the validations for segmentation are performed at both the 2D vessel cross-section segmentation and the final, whole 3D blood vessel segmentation. Various measurements taken for validating 2D and 3D segmentation are,

$$\text{Dice coefficient} = \frac{2TP}{2TP + FN + FP} \quad (11)$$

$$\text{Sensitivity} = \frac{TP}{TP + FN} \quad (12)$$

$$\text{Specificity} = \frac{TN}{FP + TN} \quad (13)$$

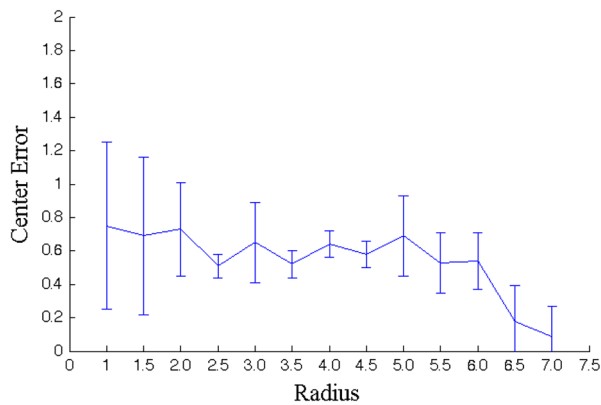


FIGURE 7. Mean center error at various radius and its standard deviation between images.

$$\text{Precision} = \frac{TP}{TP + FP} \quad (14)$$

where TP is true positives, FP is false positives, TN is true negatives and FN is false negatives. The Dice coefficient, which is same as the F1 score, is a widely used similarity measurement between two segmentations.

2D ground-truth vessel cross-section images for validation are obtained by interpolating 3D ground-truth at positions corresponding to the positions of 2D cross-section images calculated in our proposed method. Table 2 shows the mean Dice coefficient, sensitivity, specificity and precision measurements, for all the 2D vessel cross-section segmentations of all four synthetic images; and their average values are $87.9\% \pm 0.9\%$, $89.2\% \pm 3.0\%$, $98.3\% \pm 0.7\%$ and $90.0\% \pm 4.0\%$, respectively.

Figure 8 shows sensitivity, specificity and precision measurements at Dice coefficients measured for 3D blood vessel segmentation of synthetic images by Frangi *vesselness*, *vesselness* with post-processing by use of active contour segmentation, our proposed method and our proposed method with post processing. For the proposed method, the measurements are given for vessel segmentation without and with the post-processing step. Our proposed method provides segmentation output with Dice coefficient of $80\% \pm 2.7\%$, without the use of post-processing. While, the validation measurements for the proposed method with post-processing step are, $94\% \pm 2.4\%$ for the Dice coefficient, $88.7\% \pm 4.0\%$ for sensitivity, 99.9% for specificity and 99.9% for precision.

TABLE 2. Mean of Dice coefficient, sensitivity, specificity and precision, calculated along all the 2D cross-section images of synthetic images.

Data	Measurements (%)	2D cross-section segmentation
Image1	Dice	87.4
	Sensitivity	90.0
	Specificity	98.1
	Precision	88.8
Image2	Dice	87.2
	Sensitivity	92.6
	Specificity	97.4
	Precision	84.9
Image3	Dice	87.9
	Sensitivity	85.2
	Specificity	98.9
	Precision	93.6
Image4	Dice	89.4
	Sensitivity	89.0
	Specificity	98.7
	Precision	92.8

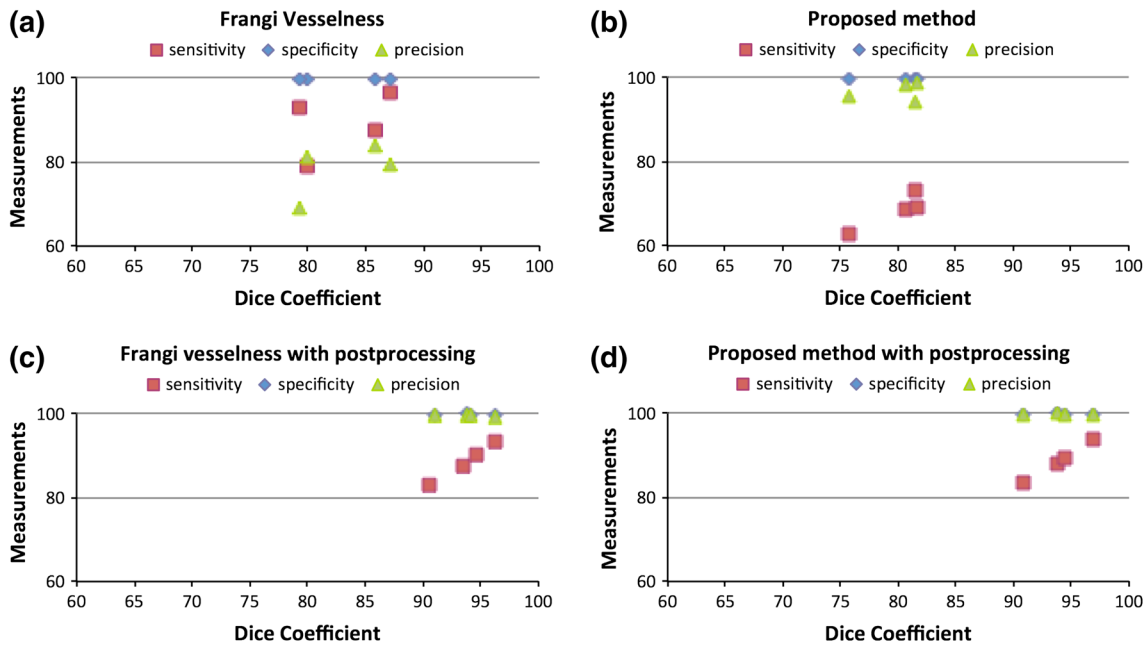


FIGURE 8. Sensitivity, specificity and precision measurements with different Dice coefficients calculated for the whole 3D blood vessel segmentation performed using (a) Frangi *vesselness* method, (b) proposed method, (c) Frangi *vesselness* with post-processing, and (d) proposed method with post-processing.

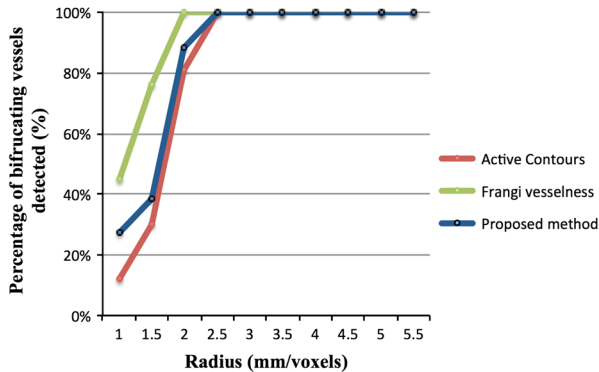


FIGURE 9. Percentage of bifurcating vessels detected by active contour segmentation, Frangi *vesselness* method with maximum entropy thresholding, and our proposed method at various vessel radius.

Bifurcating Vessel Detection

Since the segmentation validation is performed only for the synthetic images, a bifurcating vessel detection study is performed for validating the proposed method on medical images. For medical images, it is important to know the percentage of detection of bifurcating vessels to understand how the proposed method performs as the radius of the bifurcating vessel reduces.

Figure 9 shows the percentage of bifurcating vessels detected as radius of the bifurcating vessels increases from 1 mm. The study is performed first by counting the total number of bifurcating vessels, and then by identifying the number of bifurcating vessels that were segmented by active contour segmentation, Frangi

vesselness method with maximum entropy thresholding, and our proposed method, at different vessel radius. The results show that the percentage of vessels detected is 100% at and above radius of 2.5 voxels for our proposed. However, the percentage of vessel detection reduces as the radius of vessel falls below 2 voxels for all the methods.

DISCUSSION

We have presented a semi-automatic algorithm for segmentation of blood vessels and extraction of their centerlines. The algorithm segments blood vessels from single user-initialized seed, and works by analyzing vessel cross-sections and tracking them to the ends of the connected blood vessel tree.

The proposed method was tested on eight image datasets, in which four were synthetic images and four were medical images. With the use of these datasets, the proposed method was validated for centerline and segmentation accuracy, as well as for processing time.

For the centerline validation, the center calculated by the proposed method at each vessel cross-section was compared to its geometric center. One pixel is the minimum center error that can occur at each vessel cross-section. Figure 7 shows that the mean center error found for all the vessel cross-sections is 0.55 pixels, which proves that the mean center error for the proposed method is half of the individual minimum. The figure also shows that the center error is lesser at

the odd diameter cross-sections than its adjacent even diameter cross-sections. This is due to the discrete nature of the image pixelization, where the odd diameters give a single specific pixel as its center whereas the even diameters can give multiple center candidates.

We performed segmentation validation for both 2D vessel cross-section segmentation and 3D connected blood vessel segmentation. In the proposed method, the 2D vessel cross-section segmented images are combined to form the final 3D blood vessel segmentation. Thus accurate 2D segmentation of vessel cross-section is important for the final 3D blood vessel segmentation. Our results in Table 2 confirm a correct 2D segmentation with an average Dice coefficient of $87.9\% \pm 0.9\%$ and precision in segmentation with $90.0\% \pm 4.0\%$.

The segmentation validation for 3D blood vessel segmentation is performed for the proposed method without and with the use of post-processing, and the Frangi *vesselness* method without and with the use of post-processing. Figure 8 shows that the Dice coefficient is similar for the Frangi *vesselness* method with an average of $83\% \pm 4.0\%$, and our proposed method with an average of $80\% \pm 2.7\%$. However, the segmentations differ as our proposed method has more false positives and less false negatives than the Frangi *vesselness* method. This is proven by the higher precision of $96.8\% \pm 1.9\%$ for the proposed method compared to $78.4\% \pm 6.5\%$ for Frangi *vesselness* method, and lower sensitivity of $68.4\% \pm 4.3\%$ for the proposed method compared to $88.9\% \pm 7.6\%$ for Frangi *vesselness* method. Lower sensitivity for the proposed method is due to the gaps in vessel segmentation, particularly at areas where there is a sudden change in the vessel-tracking angle and also at bifurcations where there is a bigger shift in seed positions. These gaps could later be filled with the use of the post-processing step and our results show that the proposed method with post-processing gives a better segmentation with Dice coefficient of $94\% \pm 2.5\%$. However, similar Dice coefficient of $93.7\% \pm 2.4\%$ can also be obtained by using the post-processing step on Frangi *vesselness* method, which shows that the high similarity measures for the segmentation results are actually obtained by the use of the post-processing step, i.e., active contours.

In synthetic images, the measurements show that the segmentation from the user-initiated active contour segmentation alone is similar to the proposed method with the post-processing step. However, on visual evaluation of medical images and from results shown in Fig. 9, segmentation by active contour method detects fewer bifurcations than the proposed method. Thus the results from synthetic and medical images

show that by providing the segmentation result from the proposed method as the starting contour for active contour segmentation will give a fast approximation to original blood vessel image with very minimum iterations.

Figure 9 also shows that the thresholded Frangi *vesselness* segmentation results detect more vessels than both the other methods. However, the disadvantage of *vesselness* method compared to a local tracking method is that the method is applied to the whole image and it detects even blood vessels that are not connected to blood vessel of interest, as shown in Fig. 6. However, *vesselness* or a whole image analysis method has an advantage of detecting vessels that might be wrongly shown as disconnected in medical images due to contrast variation. It is also to be noted that more vessel detection could be achieved with the Frangi *vesselness* method by manually lowering the threshold, but at the cost of detecting more vessel-like structures that are not of interest.

The proposed algorithm was coded in C++ with the use of ITK libraries and the post-processing step was performed using ITK-Snap. Table 1 clearly shows that our proposed method is faster than all the compared methods for centerline extraction. The post-processing step for the proposed method took on an average only 1 s extra. The final processing time is within reasonable limits for use during intra-operative procedures, where faster update of the blood vessels is required.

A drawback of our method is in not detecting gaps and abnormalities in the blood vessels. The reason behind this is that our method while tracking always analyses the structural information of the blood vessel, which is tubular in nature for blood vessels and circular or ellipsoidal for vessel cross-sections. Another concern is at blood vessel fusion, where the blood vessels overlap due to imaging artifacts. Here, the proposed method might consider the fusion area as a bifurcation.

Figure 9 shows that the percentage of detection of bifurcating blood vessels for our proposed method falls drastically below vessel radius of 2 mm/voxels. However, for medical applications such as liver resection, blood vessels with a radius below 2 mm are not of interest.

In conclusion, we have presented a fast method for simultaneous blood vessel segmentation and centerline extraction. The novelty of our method is in performing only two-dimensional cross-section analysis for segmentation of connected blood vessels from a single user-initialized seed point. Our method also has the potential to be used for simultaneous blood vessel segmentation and labeling, for example in visualizing liver blood vessels separately as hepatic and portal system. In the future work, we will work on extending

our algorithm to segment more complex blood vessel structure like trifurcations, which are particularly useful for blood vessel segmentation in liver. We will also work on detecting small gaps in the connected blood vessels with an angle based search at the end points and on detecting abnormalities such as aneurysms in blood vessels by incorporating blob detection when the tracking reaches an abnormal structure. Our future work will also include detection of overlap and limit the leaking at these areas by including a vessel direction based restriction.

ACKNOWLEDGMENTS

The research leading to these results has received funding from the European Community's Seventh Framework Programme (FP7/2007-2013) under Grant Agreement Number 238802 (IIOS project) and also, received top-up financing from Norwegian Research Council. The authors thank Mr. Martin Rube and Prof. Andreas Melzer from the Institute of Medical Sciences and Technology, University of Dundee for providing the images necessary for our study. The authors also thank Mr. Rafael Palomar for proof-reading the document.

REFERENCES

- ¹Abd-Almageed, W., C. E. Smith, and S. Ramadan. Kernel snakes: non-parametric active contour models, Vol. 1. IEEE International Conference on Systems, Man and Cybernetics, 2003. 2003, pp. 240–244.
- ²Albregtsen, F. Non-parametric histogram thresholding methods-error vs. relative object area. Proceedings of the Scandinavian Conference on Image Analysis. 1993, p. 12.
- ³Canny, J. A computational approach to edge detection. *IEEE Trans. Pattern Anal. Mach. Intell.* PAMI-8:679–698, 1986.
- ⁴Erdt, M., M. Raspe, and M. Suehling. Automatic hepatic vessel segmentation using graphics hardware. *Medical Imaging and Augmented Reality*. Springer, Berlin, 2008, pp. 403–412.
- ⁵Frangi, A. F., W. J. Niessen, K. L. Vincken, and M. A. Viergever. Multiscale vessel enhancement filtering. *Medical Image Computing and Computer-Assisted Intervention—MICCAI'98*. Springer, 1998, pp. 130–137.
- ⁶Galarreta-Valverde, M. A., M. M. Macedo, C. Mekkaoui, and M. P. Jackowski. Three-dimensional synthetic blood vessel generation using stochastic L-systems. *SPIE Medical Imaging*. 2013, pp. 86691I-1–86691I-6.
- ⁷Kapur, J. N., P. K. Sahoo, and A. K. C. Wong. A new method for gray-level picture thresholding using the entropy of the histogram. *Comput. Vis. Graph. Image Process.* 29:273–285, 1985.
- ⁸Kass, M., A. Witkin, and D. Terzopoulos. Snakes: active contour models. *Int. J. Comput. Vis.* 1:321–331, 1988.
- ⁹Kirbas, C., and F. K. Quek. Vessel extraction in medical images by 3D wave propagation and traceback. *Proceedings of the Third IEEE Symposium on Bioinformatics and Bioengineering*, 2003, pp. 174–181.
- ¹⁰Kirbas, C., and F. Quek. A review of vessel extraction techniques and algorithms. *ACM Comput. Surv. CSUR* 36:81–121, 2004.
- ¹¹Krissian, K., G. Malandain, N. Ayache, R. Vaillant, and Y. Troussset. Model-based detection of tubular structures in 3D images. *Comput. Vis. Image Underst.* 80:130–171, 2000.
- ¹²Kumar, R. P., F. Albregtsen, M. Reimers, T. Langø, B. Edwin, and O. J. Elle. 3D multiscale vessel enhancement based centerline extraction of blood vessels. *SPIE Medical Imaging*. International Society for Optics and Photonics, 2013, pp. 86691X-1–86691X-9.
- ¹³Kumar, R. P., E.-J. Rijkhorst, O. Geier, D. Barratt, and O. J. Elle. Study on liver blood vessel movement during breathing cycle. *Colour and Visual Computing Symposium (CVCS)*, IEEE, 2013, pp. 1–5.
- ¹⁴Lee, T. C., R. L. Kashyap, and C. N. Chu. Building skeleton models via 3-D medial surface axis thinning algorithms. *CVGIP Graph. Models Image Process.* 56:462–478, 1994.
- ¹⁵Lesage, D., E. D. Angelini, I. Bloch, and G. Funka-Lea. A review of 3D vessel lumen segmentation techniques: models, features and extraction schemes. *Med. Image Anal.* 13:819–845, 2009.
- ¹⁶Lindeberg, T. Scale-space theory: a basic tool for analyzing structures at different scales. *J. Appl. Stat.* 21:225–270, 1994.
- ¹⁷Lorigo, L. M., O. D. Faugeras, W. E. L. Grimson, R. Keriven, R. Kikinis, A. Nabavi, and C.-F. Westin. CURVES: curve evolution for vessel segmentation. *Med. Image Anal.* 5:195–206, 2001.
- ¹⁸Macedo, M. M. G., M. A. Galarreta-Valverde, C. Mekkaoui, and M. P. Jackowski. A centerline-based estimator of vessel bifurcations in angiography images. In: *SPIE Medical Imaging*, International Society for Optics and Photonics, edited by C. L. Novak and S. Aylward, 2013, pp. 86703K-1–86703K-7.
- ¹⁹Maksimovic, R., S. Stankovic, and D. Milovanovic. Computed tomography image analyzer: 3D reconstruction and segmentation applying active contour models—“snakes”. *Int. J. Med. Inf.* 58–59:29–37, 2000.
- ²⁰Reinertsen, I., M. Descoteaux, K. Siddiqi, and D. L. Collins. Validation of vessel-based registration for correction of brain shift. *Med. Image Anal.* 11:374–388, 2007.
- ²¹Sato, Y., S. Nakajima, N. Shiraga, H. Atsumi, S. Yoshida, T. Koller, G. Gerig, and R. Kikinis. Three-dimensional multi-scale line filter for segmentation and visualization of curvilinear structures in medical images. *Med. Image Anal.* 2:143–168, 1998.
- ²²Schmitt, H., M. Grass, V. Rasche, O. Schramm, S. Haehnel, and K. Sartor. An X-ray-based method for the determination of the contrast agent propagation in 3-D vessel structures. *IEEE Trans. Med. Imaging* 21:251–262, 2002.
- ²³Yi, J., and J. B. Ra. A locally adaptive region growing algorithm for vascular segmentation. *Int. J. Imaging Syst. Technol.* 13:208–214, 2003.
- ²⁴Yushkevich, P. A., J. Piven, H. C. Hazlett, R. G. Smith, S. Ho, J. C. Gee, and G. Gerig. User-guided 3D active contour segmentation of anatomical structures: significantly improved efficiency and reliability. *NeuroImage* 31:1116–1128, 2006.